

Nodal pair-density-waves from quarter-metal in crystalline graphene multilayers

Sk Asrap Murshed,^{1,*} András L. Szabó,^{2,*} and Bitan Roy¹

¹*Department of Physics, Lehigh University, Bethlehem, Pennsylvania, 18015, USA*

²*Institute for Theoretical Physics, ETH Zürich, 8093 Zürich, Switzerland*

(Dated: October 28, 2022)

Crystalline graphene heterostructures, namely Bernal bilayer and rhombohedral trilayer graphene, subject to electric displacement fields, display a rich confluence of competing orders, resulting in a valley-degenerate, spin-polarized half-metal at moderate doping, and a spin- and valley-polarized quarter-metal at low doping. Here we show that the annular Fermi surface of such a quarter-metal can be susceptible toward the nucleation of a unique spin and valley polarized superconducting state, accommodating interlayer Cooper pairs that break the translational symmetry, giving rise to a Kekulé or columnar pair-density-wave. The superconducting ground state produces isolated Fermi pockets of neutral Majorana fermions, featuring a three-fold rotational symmetry, resulting in power-law scaling physical observables with temperature (T), such as specific heat $C_v \sim T$.

Introduction. At the dawn of twentieth century, a series of pioneer experiments by Kamerlingh Onnes unearthed a novel quantum phase of matter in ordinary metals that shows zero electrical resistance below a few Kelvins: Superconductors. Almost half a century later, successful microscopic theory of superconductivity by Bardeen, Cooper and Schrieffer, spurred a new wave of scientific investigations in this direction [1, 2]. Since then material realizations of high- T_c , nodal, time-reversal odd, mixed parity and topological superconductors have enriched this landscape [3–6]. From this jammed crowd, one member takes the center stage, Fulde-Farrell-Larkin-Ovchinnikov (FFLO) superconductors, as the constituting Cooper pairs break the translational symmetry [7, 8]. When periodic modulations of the Cooper amplitude is commensurate with the underlying enlarged lattice periodicity, a special class of FFLO pairing emerges: Pair-density-wave (PDW) [9–15].

Nodal superconductors are fascinating as they harbor gapless neutral Bogoliubov de-Gennes (BdG) quasiparticles, typically around point or line nodes [16, 17]. Nevertheless, an intriguing alternative, involving gapless BdG quasiparticles existing over an extended regime in the Brillouin zone, is also possible. It gives rise to the notion of inflated nodes and Majorana-Fermi surfaces [18–25].

Here we show that a spin and valley nondegenerate quarter-metal (QM) phase in multilayer graphene heterostructures host a conducive podium where a marriage between PDW and inflated nodal superconductivity, featuring isolated Majorana-Fermi pockets, can take place. The spatial modulation of such PDWs are shown in Fig. 1 and the resulting gapless Majorana-Fermi pockets are displayed in Fig. 2. Our findings are particularly pertinent in Bernal bilayer graphene (BBLG) and rhombohedral trilayer graphene (RTLG), where such a QM has been observed experimentally [26–30].

Background & motivation. Electronic bands in graphene heterostructures possess four-fold valley and spin degeneracy. On the other hand, experimentally observed global phase diagrams of BBLG and RTLG, sub-

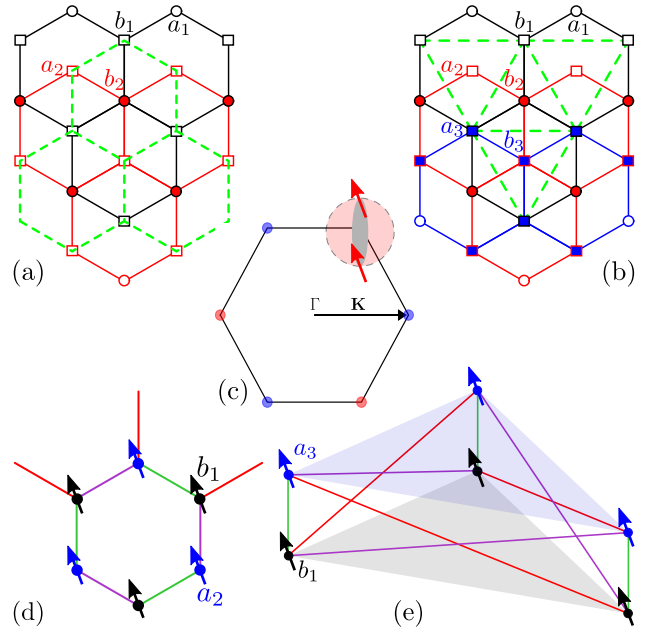


FIG. 1. Top view of (a) BBLG and (b) RTLG. Split-off bands at high energies reside predominantly on the overlapping sites, namely a_1, b_2 in BBLG and a_1, b_2 and a_2, b_3 in RTLG. Integration over the high energy bands yields an effective low-energy two-band model on two sets of sites, which form an effective honeycomb (prismlike) lattice in BBLG (RTLG), highlighted in green. (c) PDW Cooper pair (gray) around a Fermi pocket (pink) near one particular valley. (d) Real space structure of PDW Cooper pairs on these two lattices are shown in (d) and (e), respectively, which along the green line is $\Delta \cos \alpha$, along the red/blue lines is $\Delta \cos(\alpha \pm 2\pi/3)$. Here $\Delta(\alpha)$ is the overall amplitude (internal angle) of the pairing.

ject to perpendicular displacement (D) field, showcase electronic interaction driven systematic spin and valley degeneracy lifting and formation of fractional metals. As such both systems support (a) a nondegenerate QM at low doping, (b) a spin polarized, valley degenerate half-metal at moderate doping, and (c) a spin and valley degenerate metal at large doping [26–30]. Furthermore, in

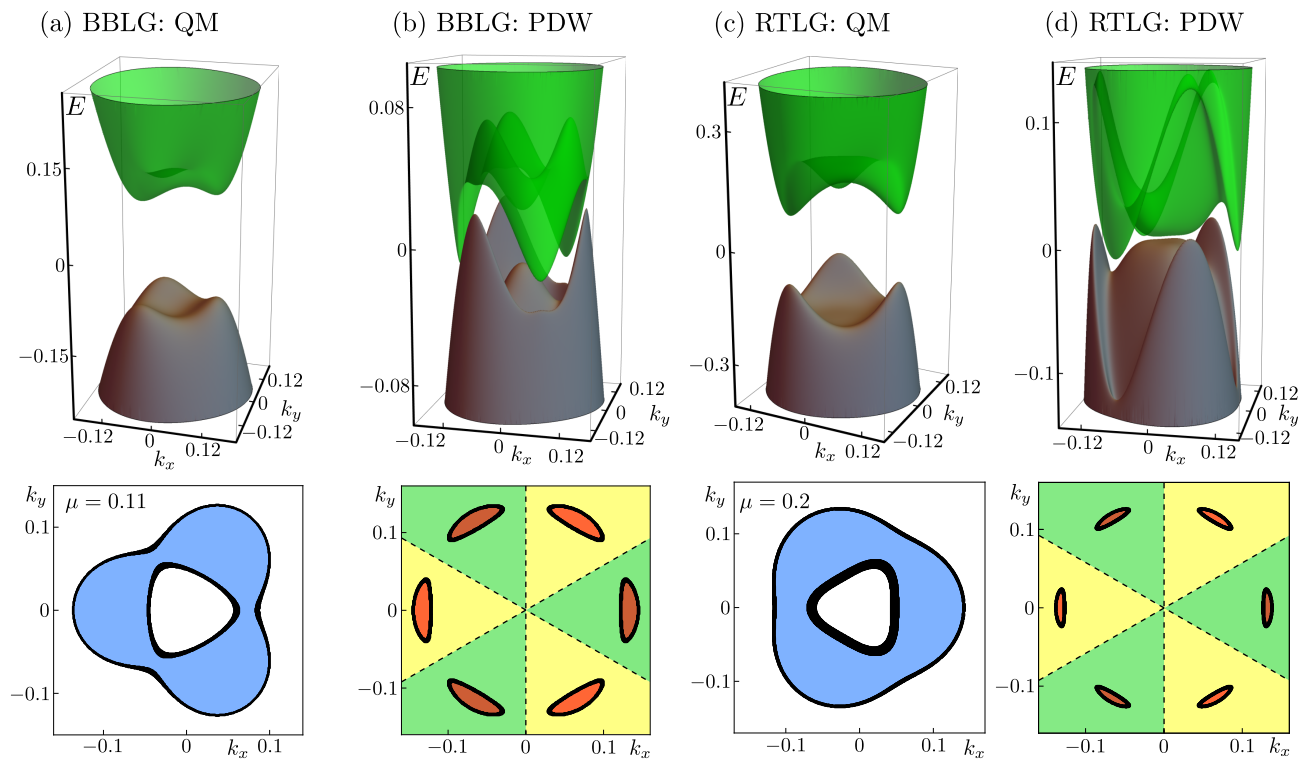


FIG. 2. Band structure (top) and Fermi surfaces (bottom) of a QM in the absence [(a) and (c)] and presence [(b) and (d)] of a PDW. Normal state electronic band structures of a QM in (a) BBLG for $t_{\perp} = 0.15$, $t_3 = 0.22$, $V = 0.15$, $m_0 = 0.12$ and (c) RTLG for $t_{\perp} = 0.2$, $t_3 = 0.05$, $V = 0.25$, $m_0 = 0.2$. Band structure of BdG fermions in (b) BBLG for $\Delta = 0.08$, $\mu = 0.11$ and (d) RTLG $\Delta = 0.06$, $\mu = 0.2$, keeping rest of the parameters from panels (a) and (c), respectively, unchanged. Here Δ is the PDW amplitude. For a small doping μ [values mentioned explicitly in (a) and (c), bottom row], the normal state QM in both systems supports annular Fermi surface (blue regions). The PDW gaps out such annular Fermi surfaces, producing isolated Majorana pockets (red regions) in the zero energy plane (charge conjugation symmetry). Due to artificial Nambu doubling, Majorana pockets only in the yellow or green regions are pertinent, connected by 3-fold rotations. Here momentum \mathbf{k} (in units of a^{-1} , where a is the lattice spacing) is measured about a specific valley at momentum $+\mathbf{K}$. Throughout we set $t = 1$.

the proximity to the half-metal superconducting phases have been observed, with, however, an assistance from a weak in-plane magnetic field in BBLG [26, 30]. Due to the spin-polarized nature of carriers in the half-metal, this paired state can only be spin-triplet, devoid of the Pauli limiting in-plane magnetic fields.

Surge of theoretical works [31–47] strongly suggests that the triplet paired state is possibly f -wave in nature, either mediated by repulsive Coulomb interactions in the spirit of the Kohn-Luttinger mechanism [33–39, 46, 47] or optical phonons [31, 45]. Although no superconductivity near the QM has been observed yet, its spin and valley polarization gives rise to fascinating possibilities. Firstly, valley and spin polarized quasiparticles when condense into Cooper pairs they give rise to a unique superconducting ground state that assumes a spatially periodic structure of periodicity $2\mathbf{K}$, where \mathbf{K} is the valley momentum, exemplifying a PDW on crystalline honeycomb heterostructures. In the ordered phase, the PDW optimally gaps the annular Fermi surface of the QM, leaving isolated gapless Majorana pockets, connected via 3-fold

rotations.

Model. We construct a minimal model involving intralayer nearest-neighbor (t) and direct interlayer (t_{\perp}) hopping. Then two out of four (six) bands in BBLG (RTLG), closest to the zero energy feature quadratic (cubic) degeneracy at two inequivalent valleys at momentum $\pm\mathbf{K}$. Here $\mathbf{K} = 4\pi(3\sqrt{3}, 0)/a$ and a is the lattice spacing. The rests, split-off bands reside at higher energies ($\sim t_{\perp}$) [48]. The fermion operators that encompass all these degrees of freedom read $\Psi = [c_{a_1}, c_{b_2}, c_{b_1}, c_{a_2}]^{\top}$ and $\Psi = [c_{a_1}, c_{b_3}, c_{a_2}, c_{b_1}, c_{a_3}, c_{b_2}]^{\top}$ for BBLG and RTLG, respectively. Here c_{sl} is a fermion annihilation operator on sublattice $s = a, b$ and layer $l = 1, 2$ (BBLG) or $l = 1, 2, 3$ (RTLG). The split-off bands dominantly reside on the pairs of overlapping sites, namely b_1 and a_2 in BBLG, and b_1 and a_2 , as well as b_2 and a_3 in RTLG [Fig. 1(a) and (b)]. The gapless bands live on the remaining two set of sites in both systems. The direct hopping with amplitude t_3 between them gives rise to trigonal warping. It splits quadratic (cubic) touching point into four (three) Dirac points in a C_3 symmetric manner, thereby preserv-

ing local nodal topology near each valley. The effect of D -field is taken into account in terms of the on-site potential V , which appears with opposite signs on the top and bottom layers. In the middle layer of RTLG $V = 0$.

With the above considerations the general Hamiltonian takes the block matrix form

$$H = \begin{pmatrix} H_{LL} & H_{LH} \\ H_{HL} & H_{HH} \end{pmatrix}, \quad (1)$$

where H_{LL} (H_{HH}) is the Hamiltonian within the subspace of only the low (high) energy sites, while H_{LH} and H_{HL} capture the coupling between them with $H_{HL} = H_{LH}^\dagger$. While for BBLG $H_{LH} = \text{diag.}(t\gamma^*, t\gamma)$,

$$H_{LL} = \begin{pmatrix} V & t_3\gamma \\ t_3\gamma^* & -V \end{pmatrix}, \quad \text{and} \quad H_{HH} = \begin{pmatrix} V & t_\perp \\ t_\perp & -V \end{pmatrix}, \quad (2)$$

with $\gamma \equiv \gamma(\mathbf{q}) = \sum_{i=1}^3 \exp[i\mathbf{q} \cdot \boldsymbol{\delta}_i]$, where \mathbf{q} is the lattice momentum, and $\boldsymbol{\delta}_1 = -a(\sqrt{3}, 1)/2$, $\boldsymbol{\delta}_2 = a(\sqrt{3}, -1)/2$ and $\boldsymbol{\delta}_3 = a(0, 1)$ are the nearest-neighbor lattice vectors, for RTLG

$$H_{LL} = \begin{pmatrix} V & t_3 \\ t_3 & -V \end{pmatrix}, \quad H_{HH} = \begin{pmatrix} 0 & t_\perp & 0 & t\gamma^* \\ t_\perp & V & 0 & 0 \\ 0 & 0 & -V & t_\perp \\ t\gamma & 0 & t_\perp & 0 \end{pmatrix},$$

and $H_{LH} = \begin{pmatrix} 0 & t\gamma^* & 0 & 0 \\ 0 & 0 & t\gamma & 0 \end{pmatrix}$. (3)

Notice that two low energy triangular sublattices constitute a honeycomb (prismlike) lattice in BBLG (RTLG). See Fig. 1(a) and (b). Therefore, the trigonal warping is devoid of any momentum dependence in RTLG.

To capture the low-energy band structure of these systems we integrate out the split-off bands or equivalently the high-energy sites. The renormalized Hamiltonian describing an effective two-band model is given by $H_{\text{ren}} = H_{LL} - H_{LH} H_{HH}^{-1} H_{HL}$ [49, 50], leading to

$$H_{\text{ren}} = \begin{pmatrix} m(\mathbf{q}) & \alpha^*(\mathbf{q}) \\ \alpha(\mathbf{q}) & -m(\mathbf{q}) \end{pmatrix}, \quad (4)$$

where for BBLG

$$m(\mathbf{q}) = V \left[1 - \frac{|\gamma|^2}{t_\perp^2 + V^2} \right], \quad \alpha(\mathbf{q}) = t_3\gamma^* - \frac{t_\perp\gamma^2}{t_\perp^2 + V^2}, \quad (5)$$

and for RTLG

$$m(\mathbf{q}) = V \left[1 - \frac{|\gamma|^4}{t_\perp^4 + V^2|\gamma|^2} \right], \quad \alpha(\mathbf{q}) = t_3 + \frac{t_\perp^2\gamma^3}{t_\perp^4 + V^2|\gamma|^2}. \quad (6)$$

The low-energy model near each valley can now be obtained by expanding H_{ren} around it, about which more in a moment. Due to the low atomic number of carbon the spin-orbit coupling in graphene heterostructures is negligible, and inclusion of spin degrees of freedom leads to mere doubling of the noninteracting Hamiltonian H_{ren} .

Coefficient	BBLG	RTLG
α_0	0	$t_3 + \frac{81}{32} \frac{1}{t_\perp^2} \mathbf{k} ^4 a^4$
α_1	$-\frac{3}{2} t_3 a$	0
α_2	$\frac{3}{8} t_3 a^2 - \frac{9}{4} \frac{t_\perp a^2}{t_\perp^2 + V^2}$	0
α_3	$\frac{3}{16} t_3 a^3 + \frac{9}{8} \frac{t_\perp a^3}{t_\perp^2 + V^2}$	$-\frac{27}{8} \frac{a^3}{t_\perp^2}$
α_{12}	$\frac{3}{8} t_3 a^3 + \frac{9}{4} \frac{t_\perp a^3}{t_\perp^2 + V^2}$	0
$m(\mathbf{k})$	$m_0 - V \frac{9}{8} \frac{2 \mathbf{k} ^2 a^2 - f_1(\mathbf{k}) a^3}{t_\perp^2 + V^2}$	$m_0 - V \frac{81}{16} \frac{1}{t_\perp^4} \mathbf{k} ^4 a^4$

TABLE I. Explicit dependence of various coefficients appearing in the effective Hamiltonian H_{QM} [Eq. (7)] for the QM in BBLG and RTLG in after the Taylor expansion around a valley at $+\mathbf{K}$ to third and fourth orders, respectively, on the hopping parameters (t_\perp , t_3), interlayer voltage bias (V) and lattice spacing (a). Here $m_0 = |V - \Delta_{\text{LAF}} - \Delta_{\text{QAH}}|$, where Δ_{LAF} (Δ_{QAH}) is the amplitude of the layer antiferromagnet (quantum anomalous Hall) order, and $f_1(k) = k_x^3 - 3k_x k_y^2$.

Competing orders & fractional metals. Fractional (half and quarter) metals stem from the simultaneous presence of multiple competing orders, for which the corresponding matrix operators commute with each other [36, 46]. The D -field induces a sublattice or equivalently a layer polarization of average electronic density, captured by $m(\mathbf{q})$. On the other hand, on-site Hubbard repulsion driven layer antiferromagnet (Δ_{LAF}) results in staggered pattern of electronic spin between the sublattices or layers [51]. The matrix operators for these two orders commute, and their simultaneous presence lifts the spin-degeneracy from electronic band, leaving their valley degeneracy unaffected. A suitable choice of chemical doping then gives rise to a spin-polarized half-metal.

While on-site repulsion is the dominant short-range interaction in graphene-based systems [52], the next relevant component of Coulomb repulsion in BBLG and RTLG subject to D field is the intralayer next-nearest-neighbor repulsion. In a spin-polarized band structure it induces quantum anomalous Hall order (Δ_{QAH}) [51]. This mass order induces a net Berry curvature by polarizing the two valleys of opposite Berry phase, and features intrasublattice circulating currents. Hence the corresponding matrix operator is diagonal in both valley and sublattice spaces, and commutes with those for layer polarized and layer antiferromagnet orders. Concomitantly, nucleation of quantum anomalous Hall order in a spin-polarized half-metal lifts the remaining valley degeneracy, giving birth to a QM at low chemical doping. It should be noted that interlayer nearest-neighbor Coulomb repulsion results in a layer polarization of electronic density. This symmetry is, however, already broken by the D field.

Quarter-metal & effective model. To capture the quintessential properties of the valley- and spin-polarized QM, next we Taylor expand H_{ren} around one particular

valley at $+\mathbf{K}$. To capture the three-fold rotational symmetry in the presence of the trigonal warping, as well as the D -field induced annular Fermi surfaces, it is necessary to expand H_{ren} up to third (fourth) order in BBLG (RTLГ). The low-energy Hamiltonian then reads

$$H_{\text{QM}} = \alpha_0 \beta_1 + \sum_{j=1,2} [\alpha_1 p_j - (-1)^j (\alpha_2 d_j + \alpha_3 f_j)] \beta_j + \alpha_{12} d_2 (p_2 \beta_1 + p_1 \beta_2) + m(\mathbf{k}) \beta_3 - \mu \beta_0, \quad (7)$$

where μ is the chemical potential, measured from the charge neutrality. Pauli matrices $\{\beta_\nu\}$ with $\nu = 0, \dots, 3$ operate on the low-energy sites. The coefficients $\alpha_{0,1,2,3}$ and α_{12} are shown in Table I. In H_{QM} we suppress the momentum dependence of the p -wave, d -wave and f -wave harmonics, respectively given by $\mathbf{p} = (k_x, k_y)$, $\mathbf{d} = (k_x^2 - k_y^2, 2k_x k_y)$ and $\mathbf{f} = (k_x^3 - 3k_x k_y^2, -k_y^3 + 3k_x^2 k_y)$, which are proportional to $Y_l^{-l} \pm Y_l^l$ combination of spherical harmonics with $l = 1, 2$ and 3 . Momentum \mathbf{k} is measured from the valley at $+\mathbf{K}$. Notice that $m(\mathbf{k})$ represents a momentum-dependent Semenofflike mass, that opens a gap near the charge neutrality point [53]. Due to the requisite simultaneous presence of layer polarization, layer antiferromagnet and quantum anomalous Hall orders to realize a nondegenerate QM, its momentum independent component is given by $m(0) = m_0 = |V - \Delta_{\text{LAF}} - \Delta_{\text{QAH}}|$. See Supplemental Materials for details [54].

By contrast, momentum dependence of $m(\mathbf{k})$ solely originates from the split-off band projection in the presence of the D field. As result, $m(\mathbf{k})$ changes sign at some momentum $|\mathbf{k}|$, thereby yielding an *annular* Fermi surface in the normal state when a *small* chemical potential places the Fermi energy within the valence or conduction band. In Figs. 2(a) and (c), we depict such annular Fermi surfaces in BBLG and RTLГ, respectively. If, on the other hand, we introduce effects of displacement field after the band projection, then $m(\mathbf{k})$ becomes momentum independent. It then produces a uniform mass gap near the charge neutrality, resulting in a simply connected regular Fermi surface upon doping.

Pair-density-wave. As a consequence of the QM being valley- and spin-polarized, the only available channel for electrons to condense into Cooper pairs is intra-valley and spin-triplet in nature. Intra-valley Cooper pairs are formed by electrons carrying opposite momentum ($+\mathbf{k}$ and $-\mathbf{k}$) with respect to the valley momentum \mathbf{K} , resulting in a center of mass momentum \mathbf{K} . The sole available pairing channel arising from the QM is therefore a commensurate FFLO or a PDW. To formally incorporate superconductivity we introduce a Nambu basis as $\Psi_{\mathbf{k}}^N = [\Psi_{\mathbf{k}}, \Psi_{-\mathbf{k}}^*]^\top$, where $\Psi_{\mathbf{k}} = [c_{\mathbf{k},a}, c_{\mathbf{k},b}]^\top$ is a two-component spinor describing electrons in the effective low-energy theory and we suppress the redundant layer index. The corresponding BdG Hamiltonian reads

$$H_{\text{BdG}} = \text{diag}[H_{\text{QM}}(\mathbf{k}), -H_{\text{QM}}^\top(-\mathbf{k})] + H_{\text{pair}}. \quad (8)$$

Here $H_{\text{pair}} = \Delta(\eta_1 \cos \phi + \eta_2 \sin \phi)M$ is the pairing Hamiltonian with amplitude Δ and superconducting $U(1)$ phase ϕ . Pauli matrices $\{\eta_i\}$ operate on the Nambu sector. Due to the particle-hole symmetry in the BdG formalism M is constrained to be purely imaginary, leaving the unique choice of pairing matrix $M = \sigma_2$ [55]. Therefore, Cooper pairs are formed by combining electrons from two low-energy sublattices of BBLG and RTLГ, residing on the complementary layers.

PDW ordering on honeycomb heterostructure results in a modulation of the superconducting amplitude with a periodicity of $2\mathbf{K}$, which can only be accommodated within an enlarged unit cell containing six sites and nine bonds [9, 56, 57]. As two low-energy sites b_1 and a_2 of BBLG constitute an emergent honeycomb lattice [Fig. 1(a)], the PDW assumes the profile of Kekulé pattern [Fig. 1(c)], similar to one on monolayer graphene. By contrast, two sets of low energy sites b_1 and a_3 residing on the bottom and top layers of the RTLГ, respectively, constitute an effective prismlike lattice [Fig 1(b)]. As a consequence RTLГ harbors a *columnar* PDW. Nonetheless, in both systems the PDW preserves the 3-fold rotational symmetry. It should be noted that in contrast to pristine graphene, the PDW emerging from the spin and valley polarized QM of BBLG and RTLГ loses the concept of valley exchange symmetry (even or odd) [9].

Finally we compute the reconstructed band structure of the QM in the presence of the PDW. Recall that external D -field produces trigonally warped annular Fermi surfaces in the normal state of the QM in both systems. See Fig. 2(a) and (c). But, the Nambu doubling [Eq. (8)] artificially doubles the number of bands. Due to the reversal of momentum the trigonal warping is opposite in the hole sector, yielding an artificial 6-fold symmetry of Nambu bands. With the onset of the PDW, while such annular Fermi surfaces get maximally gapped, it also produces six gapless Majorana-Fermi pockets. See Fig. 2(b) and (d). Upon eliminating the double counting, we recognize that the inflated nodes of the PDW produce only three Majorana-Fermi pockets, connected via 3-fold rotations, as the paired state preserves the C_3 symmetry. See Fig. 1(d) and (e).

Discussions. From a unified description of the spin and valley nondegenerate QM in BBLG and RTLГ, featuring annular Fermi surfaces, here we identify a unique superconducting instability in these systems. The paired state represents a PDW in both systems and supports isolated Majorana-Fermi pockets connected via 3-fold rotations in the ordered phase. Constant density of states produced by Majorana-Fermi pockets should manifest in power-law scaling of the specific heat $C_v \sim T$, while the ratios of the longitudinal thermal conductivity (κ_{jj}) and inverse of nuclear magnetic relaxation time $1/(T_1)$ to temperature (T) approach constant values as $T \rightarrow 0$ [58, 59]. The PDW respectively assumes Kekulé and columnar shapes in BBLG and RTLГ. Experimental observation

of such novel quantum phases, however, faces a practical challenge as they require condensation of a macroscopic number of *interlayer* Cooper pairs, which can considerably lower the critical temperature. Such an inflated nodal PDW, can in principle result from longer ranged Hubbardlike repulsions, which will be studied in future. Although not experimentally pertinent, the Kekulé PDW can also condense from a QM in monolayer graphene, where it, however, represents a fully gapped state. Altogether, observed superconductivity, proximal to correlated ground states in crystalline [26–30, 60] and Moiré graphene heterostructures [61–64], along with the genuine possibility of electronic PDW in BBLG and RTLG in the low doping regime originating from the QM place us at the dawn of carbon age of superconductivity.

Acknowledgments. S.A.M and B.R. were supported by a Startup grant of B.R. from Lehigh University. A.S. was financed through the Swiss National Science Foundation (Division II Grant No. 184739).

* Equal contributors

- [1] J. R. Schrieffer, *Theory of Superconductivity* (1st Ed., Perseus Books, 1999).
- [2] M. Tinkham, *Introduction to Superconductivity* (2nd Ed., Dover Publication, 2004).
- [3] M. Sigrist and K. Ueda, *Rev. Mod. Phys.* **63**, 239 (1991).
- [4] X. Zhou, W-S. Lee, M. Imada, N. Trivedi, P. Phillips, H-Y. Kee, P. Törmä, and M. Eremets, *Nat. Rev. Phys.* **3**, 462 (2021).
- [5] G. E. Volovik, *The Universe in a Helium Droplet* (Oxford University Press, Oxford, UK, 2003).
- [6] Y. Ando and L. Fu, *Annu. Rev. Condens. Matter Phys.* **6**, 361 (2015).
- [7] P. Fulde and R. A. Ferrell, *Phys. Rev.* **135**, A550 (1964).
- [8] A. I. Larkin and Y. N. Ovchinnikov, *Zh. Eksp. Teor. Fiz.* **47**, 1136 (1964), [*Sov. Phys. JETP* **20**, 762 (1965)].
- [9] B. Roy and I. F. Herbut, *Phys. Rev. B* **82**, 035429 (2010).
- [10] D. F. Agterberg, J. S. Davis, S. D. Edkins, E. Fradkin, D. J. Van Harlingen, S. A. Kivelson, P. A. Lee, L. Radzihovsky, J. M. Tranquada, Y. Wang, *Annu. Rev. Condens. Matter Phys.* **10**, 231 (2020).
- [11] D. Shaffer, F. J. Burnell, R. M. Fernandes, arXiv:2209.14469
- [12] Y-M. Wu, P. A. Nosov, A. A. Patel, S. Raghu, arXiv:2209.09254
- [13] K. S. Huang, Z. Han, S. A. Kivelson, and H. Yao, *npj Quantum Mater.* **7**, 17 (2022)
- [14] Y. Liu, T. Wei, G. He, Y. Zhang, Z. Wang, J. Wang, arXiv:2209.04592
- [15] H. Chen, H. Yang, B. Hu, Z. Zhao, J. Yuan, Y. Xing, G. Qian, Z. Huang, G. Li, Y. Ye, S. Ma, S. Ni, H. Zhang, Q. Yin, C. Gong, Z. Tu, H. Lei, H. Tan, S. Zhou, C. Shen, X. Dong, B. Yan, Z. Wang, H.-J. Gao, *Nature (London)* **599**, 222 (2021).
- [16] G. E. Volovik and L. P. Gor'kov, *Pis'ma Zh. Éksp. Teor. Fiz.* **39**, 550 (1984) [*JETP Lett.* **39**, 674 (1984)].
- [17] G. E. Volovik and L. P. Gor'kov, *Zh. Éksp. Teor. Fiz.* **88**, 1412 (1985) [*Sov. Phys. JETP* **61**, 843 (1985)].
- [18] K. Yang and S. L. Sondhi, *Phys. Rev. B* **57**, 8566 (1998).
- [19] W. V. Liu and F. Wilczek, *Phys. Rev. Lett.* **90**, 047002 (2003).
- [20] E. Gubankova, E. G. Mishchenko, and F. Wilczek, *Phys. Rev. Lett.* **94**, 110402 (2005).
- [21] D. F. Agterberg, P. M. R. Brydon, and C. Timm, *Phys. Rev. Lett.* **118**, 127001 (2017).
- [22] P. M. R. Brydon, D. F. Agterberg, H. Menke, and C. Timm, *Phys. Rev. B* **98**, 224509 (2018).
- [23] C. Setty, S. Bhattacharyya, Y. Cao, A. Kreisell, and P. J. Hirschfeld, *Nat. Commun.* **11**, 523 (2020).
- [24] J. M. Link, I. Boettcher, and I. F. Herbut, *Phys. Rev. B* **101**, 184503 (2020).
- [25] J. M. Link and I. F. Herbut, *Phys. Rev. Lett.* **125**, 237004 (2020).
- [26] H. Zhou, Y. Saito, L. Cohen, W. Huynh, C. L. Patterson, F. Yang, T. Taniguchi, K. Watanabe, and A. F. Young, *Science* **375**, 774 (2022).
- [27] S. C. de la Barrera, S. Aronson, Z. Zheng, K. Watanabe, T. Taniguchi, Q. Ma, P. Jarillo-Herrero, and R. Ashoori, *Nat. Phys.* **18**, 771 (2022).
- [28] A. M. Seiler, F. R. Geisenhof, F. Winterer, K. Watanabe, T. Taniguchi, T. Xu, F. Zhang, and R. T. Weitz, *Nature (London)* **608**, 298 (2022).
- [29] H. Zhou, T. Xie, A. Ghazaryan, T. Holder, J. R. Ehrets, E. M. Spanton, T. Taniguchi, K. Watanabe, E. Berg, M. Serbyn, and A. F. Young, *Nature (London)* **598**, 429 (2021).
- [30] H. Zhou, T. Xie, T. Taniguchi, K. Watanabe, and A. F. Young, *Nature (London)* **598**, 434 (2021).
- [31] Y.-Z. Chou, F. Wu, J. D. Sau, and S. Das Sarma, *Phys. Rev. Lett.* **127**, 187001 (2021)
- [32] S. Chatterjee, T. Wang, E. Berg, and M. P. Zaletel, arXiv:2109.00002
- [33] A. Ghazaryan, T. Holder, M. Serbyn, and E. Berg, *Phys. Rev. Lett.* **127**, 247001 (2021).
- [34] Z. Dong and L. Levitov, arXiv:2109.01133
- [35] T. Cea, P. A. Pantaleón, V. T. Phong, and F. Guinea, *Phys. Rev. B* **105**, 075432 (2022).
- [36] A. L. Szabó and B. Roy, *Phys. Rev. B* **105**, L081407 (2022).
- [37] Y-Z. You and A. Vishwanath, *Phys. Rev. B* **105**, 134524 (2022).
- [38] D-C. Lu, T. Wang, S. Chatterjee, and Y-Z. You, *Phys. Rev. B* **106**, 155115 (2022).
- [39] W. Qin, C. Huang, T. Wolf, N. Wei, I. Blinov, A. H. MacDonald, arXiv:2203.09083
- [40] C. Huang, T. Wolf, W. Qin, N. Wei, I. Blinov, and A. H. MacDonald, arXiv:2203.12723
- [41] J. B. Curtis, N. R. Poniatowski, Y. Xie, A. Yacoby, E. Demler, and P. Narang, arXiv:2209.10560
- [42] V. Juričić, E. Muñoz, and R. Soto-Garrido, arXiv:2209.02732
- [43] A. Jimeno-Pozo, H. Sainz-Cruz, T. Cea, P. A. Pantaleón, and F. Guinea, arXiv:2210.02915
- [44] A. S. Patri and T. Senthil, arXiv:2210.08025
- [45] Y-Z. Chou, F. Wu, J. D. Sau, and S. Das Sarma, *Phys. Rev. B* **105**, L100503 (2022).
- [46] A. L. Szabó and B. Roy, *Phys. Rev. B* **105**, L201107 (2022).
- [47] Z. Dong, A. V. Chubukov, and L. Levitov, arXiv:2205.13353
- [48] A. H. Castro Neto, F. Guinea, N. M. R. Peres, K. S.

- Novoselov, and A. K. Geim, *Rev. Mod. Phys.* **81**, 109 (2009).
- [49] R. M. A. Dantas, F. Peña-Benitez, B. Roy, and P. Surówka, *Phys. Rev. Research* **2**, 013007 (2020).
- [50] A. Panigrahi, V. Juričić, and B. Roy, *Commun. Phys.* **5**, 230 (2022)
- [51] A. L. Szabó and B. Roy, *Phys. Rev. B.* **103**, 205135 (2021).
- [52] T. O. Wehling, E. Şaşıoğlu, C. Friedrich, A. I. Lichtenstein, M. I. Katsnelson, and S. Blügel, *Phys. Rev. Lett.* **106**, 236805 (2011).
- [53] G. W. Semenoff, *Phys. Rev. Lett.* **53**, 2449 (1984).
- [54] See Supplementary Materials at XXXX-XXX for the detailed derivation of the effective Hamiltonian for the QM.
- [55] The Nambu spinor is endowed with antiunitary charge conjugation symmetry under $C = \eta_1 \mathcal{K}$, where \mathcal{K} is complex conjugation. For $(\Psi_{\mathbf{k}}^N)^\dagger H_{\text{pair}} \Psi_{\mathbf{k}}^N$ to be nonvanishing H_{pair} and C have to anticommute, constraining M to be purely imaginary.
- [56] J. Zhou, T. Qin, and J. Shi, *Chin. Phys. Lett.* **30**, 017401 (2013).
- [57] S. Tsuchiya, J. Goryo, E. Arahata, and M. Sigrist, *Phys. Rev. B* **94**, 104508 (2016).
- [58] B. Roy, S. A. A. Ghorashi, M. S. Foster, and A. H. Nevidomskyy, *Phys. Rev. B* **99**, 054505 (2019).
- [59] C. J. Lapp, G. Börner, and C. Timm, *Phys. Rev. B* **101**, 024505 (2020).
- [60] . Hagymási, M. S. M. Isa, Z. Tajkov, K. Máritý, O. László, J. Koltai, A. Alassaf, P. Kun, K. Kandrai, A. Pálinkás, P. Vancsó, L. Tapasztó, P. Nemes-Incze, *Sci. Adv.* **8**, eabo6879 (2022).
- [61] Y. Cao, V. Fatemi, S. Fang, K. Watanabe, T. Taniguchi, E. Kaxiras, and P. Jarillo-Herrero, *Nature (London)* **556**, 43 (2018).
- [62] X. Lu, P. Stepanov, W. Yang, M. Xie, M. A. Aamir, I. Das, C. Urgell, K. Watanabe, T. Taniguchi, G. Zhang, A. Bachtold, A. H. MacDonald, and D. K. Efetov, *Nature (London)* **574**, 653 (2019).
- [63] M. Yankowitz, S. Chen, H. Polshyn, K. Watanabe, T. Taniguchi, D. Graf, A. F. Young, and C. R. Dean, *Science* **363**, 1059 (2019).
- [64] U. Zondiner, A. Rozen, D. Rodan-Legrain, Y. Cao, R. Queiroz, T. Taniguchi, K. Watanabe, Y. Oreg, F. von Oppen, A. Stern, E. Berg, P. Jarillo-Herrero, and S. Ilani, *Nature (London)* **582**, 203 (2020).